Towards photocatalytic water splitting in homogeneous solutions using molecular metalloporphyrin photosensitizers and catalysts

Liu, C.

4

Electronic Effects in Water-soluble Zn(II)- and Sn(IV)-Porphyrin Photosensitizers for Homogeneous Photocatalytic Hydrogen Evolution at pH 7.0

A series of tetra-anionic Zn(II)- and Sn(IV)-porphyrin complexes bearing either electron-donating ($[M\text{-}OMeP]^{4-}$, $[M\text{-}MeP]^{4-}$, M = $Sn^{IV}Cl_2$ or Zn^{II}) or electron-withdrawing ($[M\text{-}F8P]^{4-}$, $[M\text{-}F16P]^{4-}$) substituents were prepared. The role of electronic effects on the photosensitizer (PS) was studied of a homogeneous photocatalytic hydrogen evolution system using cobaloxime as hydrogen evolution catalyst (HEC), green light irradiation (550 nm), and triethanolamine (TEOA) as sacrificial electron donor in a 1:1 pH 7.0 water/acetonitrile solution. Electronic effects on the one hand fine-tune the redox properties of the ground state of the PS; on the other hand, they also affect its triplet excited state energy, which further changes the potentials of the redox couples involving the excited state of the PS. These effects appear to have an effect both on the thermodynamics of the photocatalytic hydrogen evolution reaction and on the quenching mechanism. The electron-poorest PS, $[Zn\text{-}F16P]^{4-}$, was the only zinc-based PS of this series to result in active catalytic system, leading to a high photocatalytic turnover number (PTON) of 850 after 20 h irradiation with a high maximum photocatalytic turnover frequency (PTOF) of 59 h^{-1}. In the Sn-porphyrin series the compounds $[Sn\text{-}OMeP]^{4-}$ and $[Sn\text{-}MeP]^{4-}$ both resulted in active catalytic systems, the latter being a much more efficient sensitizer than the former; both were less efficient than $[Zn\text{-}F16P]^{4-}$ in otherwise identical conditions. The best PS of these two series of complexes, $[Zn\text{-}F16P]^{4-}$, showed great photostability in optimized conditions, driving photocatalytic hydrogen evolution for more than 100 h under green light irradiation.

4.1 Introduction

Reducing the CO_2 emission originating from the use of fossil fuels is important for achieving a "carbon neutral" society. To achieve this goal, the utilization of a carbon-free replacement of fossil fuels, such as dihydrogen, is imperative and extremely urgent.[1,2] Photocatalytic hydrogen generation could convert and store superfluous solar energy into chemical energy by the production of H_2 in a sustainable and environmentally friendly manner.[2-4] The photoinduced hydrogen evolution reaction (HER) typically requires three components: a photosensitizer (PS), which is responsible for light harvesting and triggering electron transfer; a hydrogen evolving catalyst (HEC); and a sacrificial electron donor (ED), which in a full photocatalytic water splitting scheme should be replaced by an electron relay that is reduced with electrons derived from water oxidation.[5,6] Recently, efforts on developing new photocatalytic systems have mainly focused on the catalysts, while comparatively less work has been dedicated to the optimization of the photosensitizer.[2,6] However, the PS plays a significant role for solar H_2 generation, and it is as important to develop more robust and more efficient photosensitizers as it is to find stable and fast catalysts.[7-9]

Noble-metal based molecular chromophores have been well studied for homogeneous light-driven hydrogen production, in particular those based on Ru,[9,10] Ir,[11,12] Pt,[13,14] Re,[15,16] and Au[17], which have shown excellent sensitizing properties. However, these noble-metal-based photosensitizers are too expensive for use on an industrial scale due to their low natural abundance. Therefore, the development of noble-metal-free chromophores is receiving more and more attention.[18-20] Although xanthene dyes, for example Eosin Y,[21,22] Rose Bengal,[23,24] or Fluorescein,[25,26] are cheap and active, most of them only last a few hours under visible light irradiation, which drastically limits their practical applications. Next to these compounds, molecular photosensitizers based on earth-abundant metals are considered in parallel. Cu(I)-based chromophores, first reported for photocatalytic hydrogen generation by Sauvage and co-workers,[27] have recently been re-introduced and explored in great detail, and indeed demonstrate promising sensitizing properties for photocatalytic HER.[28-32] However, most of the photocatalytic systems described to date containing a Cu(I)-based PS still suffer from low photostability due to decomposition of the Cu(I) photosensitizers.[6] Improvements of the stability of these PSs and optimization of their sensitizing properties for hydrogen evolution remains necessary.

Another family of photosensitizers based on abundant metals has been considered: porphyrin-based metal complexes. These molecules not only show intense absorption of visible light due to their large conjugated ring and allowed π–π* transitions, but they also have good stability due to the tetradentate, rigid coordination environment containing the metal center.[3, 33] Porphyrin ligands can be readily functionalized with substituents for fine-tuning the electronic density of the metal centers, or for improving water solubility. This versatility allows porphyrin-based PSs to be tunable both in terms of redox and aggregation properties in aqueous media.[3,6] However, although noble-metal-free porphyrin-based PSs, and in particular those based on Zn(II) and Sn(IV), have already been considered as PS in catalytic systems for photocatalytic hydrogen production,[7,34-36] full understanding is still lacking of the effects that electronic properties of the porphyrin ligand have on their sensitizing properties and stability for the photocatalytic HER.

In the work reported in this chapter, we have prepared two series of water-soluble Zn(II)- and Sn(IV)-porphyrin complexes bearing either electron-donating ([M-OMeP]$^{4-}$, [M-MeP]$^{4-}$, M = Zn^{II} or $Sn^{IV}Cl_2$) or electron-withdrawing ([M-F8P]$^{4-}$, [M-F16P]$^{4-}$) substituents (Figure 4.1). These complexes were tested as photosensitizers for the photocatalytic HER in homogeneous 1:1 pH 7.0 water/acetonitrile (MeCN) solutions, using green light (550 nm) irradiation, cobaloxime as standard HEC, and triethanolamine (TEOA) as the ED. The synthetic availability of these two series of complexes with electron-poor or electron-rich ligands allowed for systematically evaluating the influence of electronic effects on the redox potentials and excited-state energy of the PS, and for studying how these molecular properties influence the overall kinetics of photocatalytic HER. A typical three-component system for photocatalytic hydrogen generation contains a PS, a HEC, and an ED. In this system, the excited state of the photosensitizer, PS*, can either first be reduced by the ED ("reductive quenching"), to become a reductant (PS^-) that further reduces the HEC, or behave as a reductant to first transfer an electron to the HEC ("oxidative quenching"), before being regenerated by electron donation by the ED (Figure 4.2).[2,5,6] Which quenching pathway is occurring in a particular photocatalytic system depends notoriously on the thermodynamics of its components, hence on the electron richness of the PS. For example, for reductive quenching the reduction potential of the ground state of the photosensitizer, $E_{PS,red}(PS/PS^-)$, should be more negative than the reduction potential of the HEC, $E_{HEC}(H^+/H_2)$; meanwhile, the reduction potential of the excited state of PS, $E_{PS^*,red}$ (PS^*/PS^-), should be more positive than the oxidation potential of the sacrificial electron donor $E(ED^+/ED)$. By contrast, for oxidative quenching the oxidation

potential of the ground state of the PS, $E_{PS,ox}(PS^+/PS)$, should be higher than $E(ED^+/ED)$ and the oxidation potential of the excited state of PS, $E_{PS*,ox}(PS^+/PS*)$, should be more negative than the $E_{HEC}(H^+/H_2)$. Here, we describe our study of how these thermodynamic aspects evolve when changing the electron density of the PS, in which we identified one particular complex that shows improved stability in photocatalytic conditions, compared to reported systems.

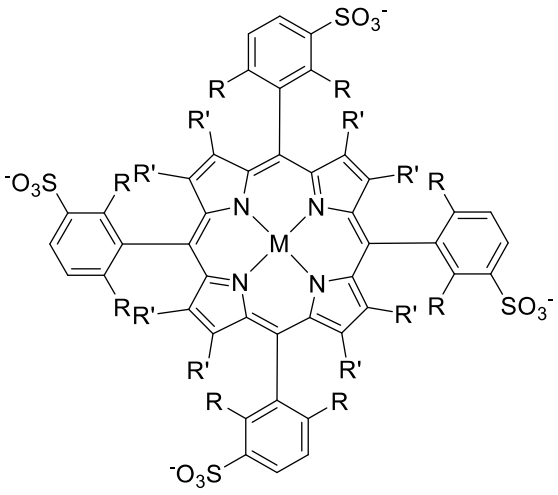

[Zn-OMeP]$^{4-}$: M = Zn^{II}, R = OCH_3, R' = H
[Zn-MeP]$^{4-}$: M = Zn^{II}, R = CH_3, R' = H
[Zn-F8P]$^{4-}$: M = Zn^{II}, R = F, R' = H
[Zn-F16P]$^{4-}$: M = Zn^{II}, R = F, R' = F
[Sn-OMeP]$^{4-}$: M = $Sn^{IV}Cl_2$, R = OCH_3, R' = H
[Sn-MeP]$^{4-}$: M = $Sn^{IV}Cl_2$, R = CH_3, R' = H
[Sn-F8P]$^{4-}$: M = $Sn^{IV}Cl_2$, R = F, R' = H
[Sn-F16P]$^{4-}$: M = $Sn^{IV}Cl_2$, R = F, R' = F

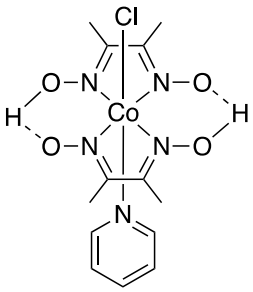

Cobaloxime

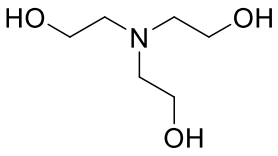

TEOA

Figure 4.1 *Chemical structures of water-soluble metal porphyrin photosensitizers reported in this work, the cobaloxime hydrogen-evolving catalyst, and the sacrificial electron donor TEOA. All porphyrin compounds were isolated as their Na^+ salts.*

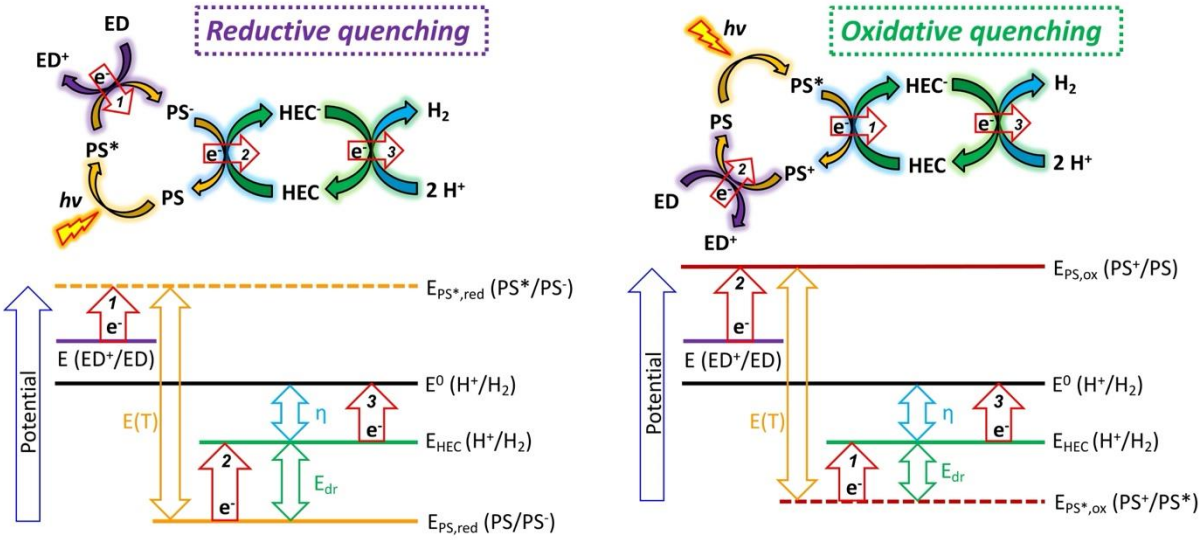

Figure 4.2 *Simplified mechanism of reductive quenching and oxidative quenching pathways and their corresponding energy schemes for three-component photocatalytic hydrogen evolution. ED: sacrificial electron donor; PS: photosensitizer; HEC: hydrogen evolving catalyst; E(T): triplet excited state energy of PS; η: overpotential of HEC; E_{dr}: driving force of the electron transfer from the photosensitizer to the catalyst.*

4.2 Results and Discussion

4.2.1 Synthesis

The tetrasulfonated free-base porphyrin ligands $Na_4[H_2\text{-OMeP}]$,[37] $Na_4[H_2\text{-MeP}]$,[38] $Na_4[H_2\text{-F8P}]$,[39] $Na_4[H_2\text{-F16P}]$,[40] and the metal complexes $Na_4[Zn\text{-F8P}]$,[41] $Na_4[Zn\text{-F16P}]$,[40] were synthesized according to reported methods. The synthesis of $Na_4[Zn\text{-OMeP}]$ and $Na_4[Zn\text{-MeP}]$ is described in **Chapter 3**. The four Sn(IV)-porphyrin compounds discussed in this chapter are new and were synthesized via refluxing the free-base ligands with Sn(II) dichloride in Milli-Q water for 12 h. An Na^+-loaded ion exchange resin was used to introduce Na^+ counter cations, and finally the Sn-porphyrin complexes were purified by size-exclusion chromatography in order to remove excess $SnCl_2$. Full characterization is given in the Supplementary Information (Figure AIII.1 - Figure AIII.6).

4.2.2 Photochemical properties

The light absorption properties of the Zn- and Sn-porphyrin complexes were studied via steady-state UV-vis measurements in 1:1 pH 7.0 water/MeCN solutions in the presence of 5% (v/v) TEOA. For both series, the intense Soret band characteristic of porphyrin ligands and

complexes was observed between 409 and 424 nm and the Q band between 540—615 nm (Figure 4.3). For both the Soret and the first Q bands, a small blue shift of the absorption peaks was found with increasing electron-withdrawing properties of the substituents, from the electron-richest $[M\text{-}OMeP]^{4-}$ to the electron-poorest $[M\text{-}F16P]^{4-}$ (M = Zn^{II} or $Sn^{IV}Cl_2$). As shown in Table 4.1, in the Zn-porphyrin series the Soret and the first Q bands shifted by 15 nm and 16 nm, respectively, while in the Sn-porphyrin series the shift was only 12 and 13 nm, respectively. From $[M\text{-}OMeP]^{4-}$ to $[M\text{-}MeP]^{4-}$, the peak shift was very limited in both series (≤ 2 nm), while from $[M\text{-}F8P]^{4-}$ to $[M\text{-}F16P]^{4-}$ and $[M\text{-}MeP]^{4-}$ to $[M\text{-}F8P]^{4-}$, the peak shift was more significant (≥ 5 nm). Overall, the electron-withdrawing substituents influenced the absorption properties of these compounds moderately.[8]

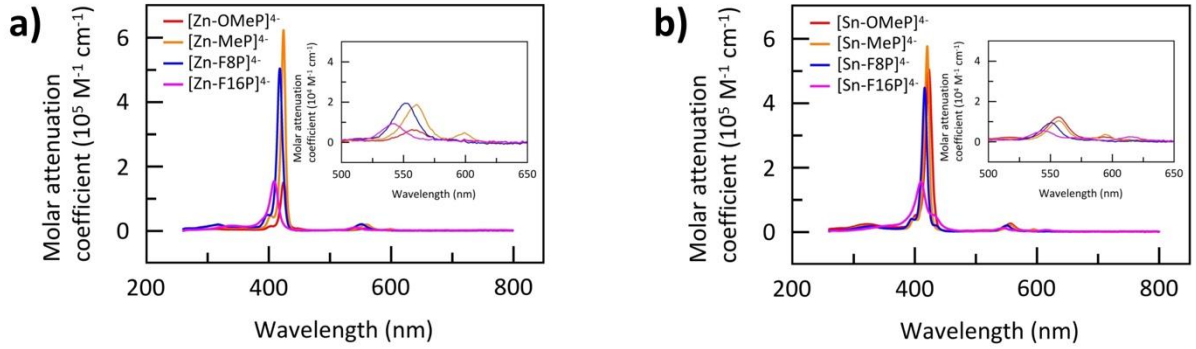

Figure 4.3 *Absorption spectra of a) Zn- and b) Sn-porphyrin complexes in 1:1 pH 7.0 water/MeCN solution under air with 5% (v/v) TEOA, T = 298 K.*

Table 4.1 *Light absorption properties of Zn- and Sn-porphyrin complexes*

	λ_{Sor}[a] (ε_{Sor}[b])	λ_{Q}[a] (ε_{Q}[b])	ε[b] at 550 nm
[Zn-OMeP]$^{4-}$	424 (140)	557 (6.4)	4.0
[Zn-MeP]$^{4-}$	424 (630)	557 (19) / 599 (4.9)	11
[Zn-*F8*P]$^{4-}$	418 (510)	551 (20)	19
[Zn-*F16*P]$^{4-}$	409 (150)	541 (10)	6.0
[*S*n-OMeP]$^{4-}$	423 (430)	557 (22) / 595 (5.0)	18
[*S*n-MeP]$^{4-}$	421 (590)	556 (19) / 595 (7.3)	15
[*S*n-*F8*P]$^{4-}$	416 (440)	551 (19)	19
[*S*n-*F16*P]$^{4-}$	411 (310)	544 (22) / 615 (4.8)	9.2

[a] λ_{Sor} and λ_{Q} are the absorption maxima (in nm) for the Soret and Q bands, respectively; both were measured in the condition of Figure 4.3.
[b] molar attenuation coefficient, $\times 10^3$ M^{-1} cm^{-1}.

4.2.3 Photocatalysis

Cobaloxime is an efficient catalyst for light-driven hydrogen evolution, which has been used as a standard HEC for photosensitizer development.[7] Unfortunately, due to its poor solubility in water it can only be used in water/MeCN mixtures. Therefore, we run all photocatalytic reactions in 1:1 water/MeCN solutions containing 5% (v/v) TEOA (~0.38 M) as sacrificial electron donor, to which HCl was added until reaching pH 7.0. The pK_a of TEOA in a 1:1 water/MeCN solution was reported to be 7.0,[7,42] we hence consider the photocatalytic solutions used in this work to be buffered at pH 7.0 by TEOA. Since all porphyrin complexes absorb 540—560 nm light (Q band), a 550 nm green LED (9 mW, >80% intensity in range 540—560 nm) was used as the light source, which allowed for comparing photocatalytic properties of the different photosensitizers. The molar attenuation coefficient of all 8 PS is

indicated in Table 4.1. Under irradiation, using 0.49 mM cobaloxime and 0.04 mM PS, [Zn-F16P]$^{4-}$ was the only compound of the Zn series to give significant photocatalytic activity (Figure 4.4a). In the Sn series, both [Sn-OMeP]$^{4-}$ and [Sn-MeP]$^{4-}$ were found to result in photoactive systems (Figure 4.4b). [Zn-F16P]$^{4-}$ showed the best efficiency of the three photosensitizers that effectively resulted in hydrogen evolution, with a photocatalytic turnover number (PTON) of 850 (mol_{H2}/mol_{PS}) after 20 h irradiation, and a maximum photocatalytic turnover frequency (PTOF, determined as explained in the Experimental Part, 4.4.5) of 59 h^{-1}. [Sn-MeP]$^{4-}$ resulted in a lower photocatalytic activity (PTON of 430 after 20 h irradiation and a maximum PTOF of 35 h^{-1}), and the photoactivity observed for [Sn-OMeP]$^{4-}$ as PS only lasted for 4 h of irradiation, with a low PTON of 30 and a low maximum PTOF of 13 h^{-1}. It is worth noting that for [Zn-F16P]$^{4-}$ in the absence of the cobaloxime HEC the photocatalytic system was not active for hydrogen evolution (Figure 4.4a). In addition, the system did not show any photocatalytic activity when replacing [Zn-F16P]$^{4-}$ by [Sn-F16P]$^{4-}$ (in the presence of cobaloxime) (Figure 4.4b). These results indicate that in the most active system using [Zn-F16P]$^{4-}$, [Zn-F16P]$^{4-}$indeed played the role of PS, even if we demonstrated in **Chapter 3** that in different conditions, and in association with $[Ru(bpy)_3]^{2+}$ as photosensitizer, it can also work as a HEC.

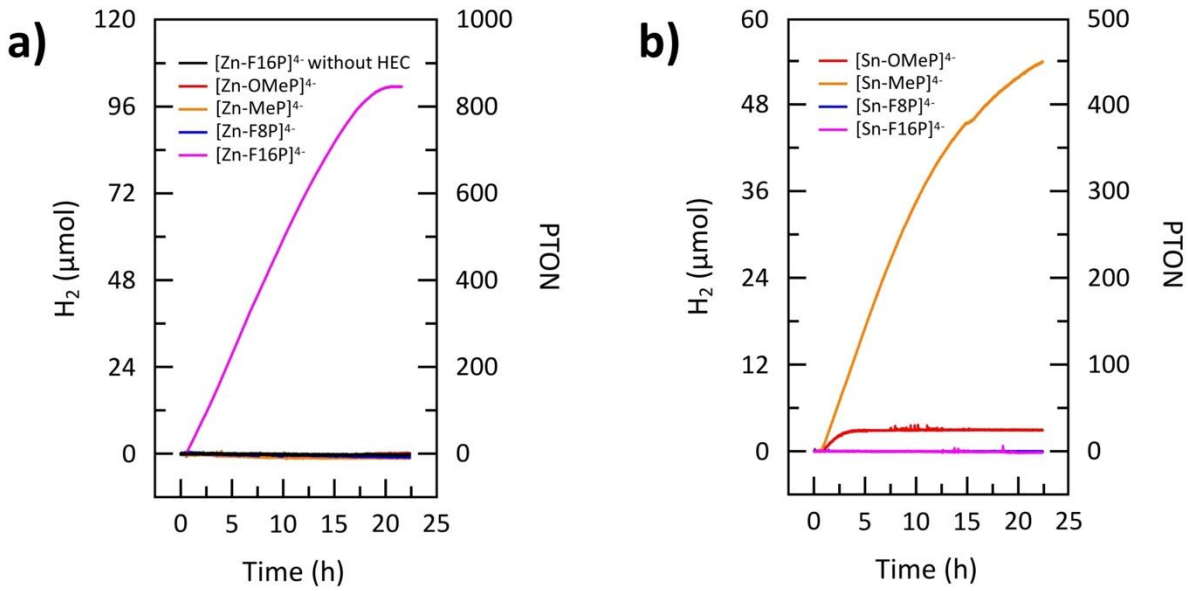

Figure 4.4 *Hydrogen evolution during photocatalytic water reduction in the presence of 0.04 mM of the photosensitizer a) [Zn-OMeP]$^{4-}$, [Zn-MeP]$^{4-}$, [Zn-F8P]$^{4-}$ and [Zn-F16P]$^{4-}$, b) [Sn-OMeP]$^{4-}$, [Sn-MeP]$^{4-}$, [Sn-F8P]$^{4-}$ and [Sn-F16P]$^{4-}$, 5% (v/v) TEOA as sacrificial electron donor, with or without (a) 0.49 mM cobaloxime as catalyst, in a 1:1 pH 7.0 water/MeCN*

solution, using green light irradiation (550 nm, 9 mW), T = 298 K. Light was switched on at t = 0.5 h.

In all cases, photocatalysis slowed down (Sn) or stopped (Zn) after ~22 h photocatalysis. Additional experiments were performed to understand whether deactivation of the most active system containing the PS $[Zn\text{-}F16P]^{4-}$ was due to the decomposition of the PS. First, 0.12 µmol of fresh $[Zn\text{-}F16P]^{4-}$ was added as solid into 3 mL of the photocatalytic mixture containing 0.04 mM $[Zn\text{-}F16P]^{4-}$, 0.49 mM cobaloxime and 5% (v/v) TEOA, after the first 22 h irradiation. When green light irradiation was resumed, no hydrogen generation was observed (Figure 4.5a). Second, when a twice higher concentration (0.08 mM) of $[Zn\text{-}F16P]^{4-}$ was used, an almost twice higher maximum PTOF (109 h^{-1}) was observed (Figure 4.4a), resulting in almost double PTON of 1690 after 20 h (Figure 4.5b). However, the lifetime of the system (~20 h) was not significantly changed. These two results strongly suggest that decomposition of the photosensitizer $[Zn\text{-}F16P]^{4-}$ is not the cause of deactivation of the photocatalytic system, and that catalyst decomposition might be the problem instead.

In a third experiment, a twice higher concentration (0.98 mM) of the cobaloxime HEC was used; the resulting photocatalytic system, still using 0.04 mM $[Zn\text{-}F16P]^{4-}$ as PS and 5% (v/v) TEOA as ED, was active this time for more than 100 h under green light irradiation (Figure 4.5c). However, the total PTON of this catalytic system after 100 h irradiation was 920, which is close to the maximum PTON 850 of the system with 0.49 mM cobaloxime after 20 h irradiation. In addition, only minor changes of the UV-vis spectra of the catalytic solution were observed after irradiating for 100 h: ~95% of the characteristic absorption peaks of $[Zn\text{-}F16P]^{4-}$ at 409 and 541 nm was retained, compared to the initial absorbance (Figure 4.5d). These results demonstrate that $[Zn\text{-}F16P]^{4-}$ has a great stability in photocatalytic conditions, and that when combined with cobaloxime as HEC, it remains photoactive at least for 100 h under green light irradiation.

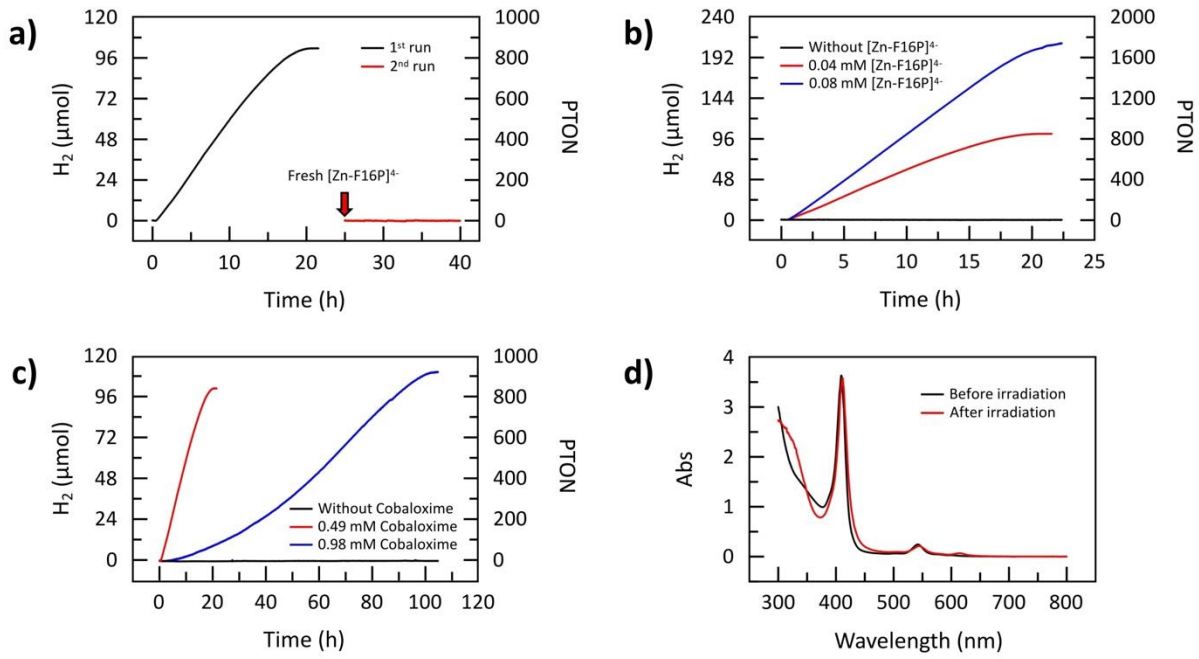

Figure 4.5 *Stability of [Zn-F16P]$^{4-}$ in photocatalytic hydrogen evolution. a) Hydrogen evolution during two consecutive photocatalytic runs, adding 1 eq. more of PS at the end of the first run. b) and c) Photocatalytic hydrogen production when doubling the initial concentration of PS (b) or that of the cobaloxime catalyst (c). d) UV-vis absorption of the photocatalytic solution used in c) before (black) and after (red) irradiation. Conditions: a) 0.04 mM [Zn-F16P]$^{4-}$, 0.49 mM cobaloxime, b) 0.04 or 0.08 mM [Zn-F16P]$^{4-}$, 0.49 mM cobaloxime, c) 0.04 mM [Zn-F16P]$^{4-}$, 0.49 or 0.98 mM cobaloxime, d) 0.04 mM [Zn-F16P]$^{4-}$, 0.98 mM cobaloxime, 5% (v/v) TEOA in 1:1 pH 7.0 water/MeCN solutions and green light irradiation (550 nm, 9 mW), T = 298 K. For all photocatalytic experiments, light was switched on at t = 0.5 h. Between the two irradiation experiments in a), 0.12 µmol fresh [Zn-F16P]$^{4-}$ was added as a solid.*

4.2.4 Electrochemical properties

In order to investigate the thermodynamics of the photocatalytic systems and the quenching mechanisms at play, the reduction and oxidation potentials of all metalloporphyrin complexes were determined using differential pulse voltammetry (DPV) measurements with a 0.07 cm^2 glassy-carbon (GC) working electrode, an Ag/AgCl reference electrode, and a Pt-wire counter electrode. As the photocatalytic experiments were always performed in a 1:1 pH 7.0 water/MeCN solution due to the poor solubility of cobaloxime in water, all the DPV measurements were performed in a 1:1 0.1 M pH 7.0 phosphate buffer/MeCN solution to mimic the photocatalytic conditions.

The photosensitizers are usually considered to accept or donate one electron at a time from or to the other components in the photocatalytic system. Therefore, in this work, we only measured the first redox potentials of all Zn- and Sn-porphyrin complexes. For the first reduction potential in the Zn porphyrin series, when going from the electron-richest complex $[Zn\text{-}OMeP]^{4-}$ to the electron-poorest $[Zn\text{-}F16P]^{4-}$ a less negative ground-state reduction potential $E_{PS,red}(PS/PS^{-})$ was found (Table 4.2 and Figure AIII.7a). In contrast, the ground-state oxidation potential $E_{PS,ox}(PS^{+}/PS)$ of the complexes were found to be more and more positive (Table 4.2 and Figure AIII.7b); only the potential of $[Zn\text{-}OMeP]^{4-}$ and $[Zn\text{-}MeP]^{4-}$ appeared to be the same. Similar trends were observed for the Sn-porphyrin series, with ground state reduction potentials of $[Sn\text{-}OMeP]^{4-}$ and $[Sn\text{-}MeP]^{4-}$ that were identical within the precision of the measurement (Table 4.2 and Figure AIII.8a), and ground state oxidation potentials that only slightly increased with the electron-withdrawing ability of the substituents (Table 4.2 and Figure AIII.8b). It is worth mentioning that, as reported by Coutsolelos and co-workers[7], the ground state oxidation potentials of the Sn(IV)-porphyrin complexes generally were found to be higher than those of the Zn(II)-porphyrin complexes. This observation probably is related to the higher oxidation state of Sn, which makes the complexes of the Sn compounds more electron poor and thus more difficult to oxidize.

4.2.5 Excited state energies

For both of the Zn- and Sn-porphyrin series, modifying the porphyrin complex with electron-withdrawing or electron-donating substituents not only changes their ground-state oxidation potential $E_{PS,ox}(PS^{+}/PS)$ and ground-state reduction potential $E_{PS,red}(PS/PS^{-})$, but also affects the Gibbs free energy of their triplet excited state, E(T). Here, we assumed that longer lifetimes are typically required in homogeneous solution to obtain a significant rate for intermolecular photoelectron transfer. Considering that the presence of a metal center in the photosensitizers increased the rate of intersystem crossing to the triplet state, we hypothesized that efficient sensitization could only take place from the triplet state (PS*) of the photosensitizer, which is longer lived than the singlet ground state (PS). E(T) was hence calculated by minimizing the geometry of the triplet state and that of the singlet ground state of each molecule using DFT, and by calculating the difference of their Gibbs free energy (Table 4.2). These DFT calculations reveal that the estimated triplet excited-state energy E(T) of the zinc(II) or tin(IV) complexes increased with the electron-withdrawing properties of the porphyrin ligand (Table 4.2), with

the exception of $[M\text{-}OMeP]^{4-}$, which showed almost identical values of E(T), compared to $[M\text{-}MeP]^{4-}$.

From these E(T) values, the potential of the redox couples involving the excited state of the photosensitizers, $E_{PS*,red}(PS*/PS^{-})$ and $E_{PS*,ox}(PS^{+}/PS*)$, were estimated (Table 4.2). The increase of the electron-withdrawing properties of the porphyrin ligand resulted in a strong increase of the ground-state reduction potential of the PS/PS^{-} couple, but also in a milder but clearly increasing triplet-state energy, which altogether led to a strongly increasing reduction potential for the $PS*/PS^{-}$ couple involving the excited triplet state. This trend leads to very positive reduction potential values $E_{PS*,red}(PS*/PS^{-})$ of +1.16 V vs. NHE for $[Zn\text{-}F16P]^{4-}$ and +1.43 V vs. NHE for $[Sn\text{-}F16P]^{4-}$), highlighting the excellent photo-oxidizing properties of these two metal porphyrin molecules. On the other hand, the increasing electron-withdrawing properties of the ligand also resulted in a strong increase of the oxidation potential of the PS^{+}/PS couple. Here, however, the already mentioned mild increase of E(T) along these two series of complexes slightly lowered the resulting increase of the oxidation potential of the $PS^{+}/PS*$ couple. For example, $E_{PS,ox}(PS^{+}/PS)$ was increased by 0.15 V from $[Sn\text{-}OMeP]^{4-}$ to $[Sn\text{-}F16P]^{4-}$, but their oxidation potentials $E_{PS*,ox}(PS^{+}/PS*)$ could not be distinguished: they were both –0.07 V vs. NHE.

Table 4.2 *Calculated triplet excited state energies and redox potentials for redox couples involving the ground state and the triplet excited state of Zn- and Sn-porphyrin complexes.*

PS	$E_{PS,red}(PS/PS^-)$[a]	$E_{PS,ox}(PS^+/PS)$[a]	E(T)[b]	$E_{PS*,red}(PS*/PS^-)$[a]	$E_{PS*,ox}(PS^+/PS*)$[a]
[Zn-OMeP]$^{4-}$	–1.18 V	0.94 V	1.69	0.51 V	–0.75 V
[Zn-MeP]$^{4-}$	–1.10 V	0.94 V	1.69	0.59 V	–0.75 V
[Zn-F8P]$^{4-}$	–0.95 V	1.20 V	1.75	0.80 V	–0.55 V
[Zn-F16P]$^{4-}$	–0.61 V	1.57 V	1.77	1.16 V	–0.20 V
[Sn-OMeP]$^{4-}$	–0.60 V	1.51 V	1.58	0.98 V	–0.07 V
[Sn-MeP]$^{4-}$	–0.60 V	1.52 V	1.53	0.93 V	–0.01 V
[Sn-F8P]$^{4-}$	–0.41 V	1.53 V	1.67	1.26 V	–0.14 V
[Sn-F16P]$^{4-}$	–0.30 V	1.66 V	1.73	1.43 V	–0.07 V

[a] V vs. NHE, as measured experimentally by DPV. Conditions: 1.0 mM PS in 1:1 (v/v) 0.1 M pH 7.0 phosphate buffer/MeCN solution, 0.07 cm^2 glassy-carbon working electrode, Pt wire auxiliary electrode, Ag/AgCl reference electrode, ±0.004 V increase potential, 0.05 V amplitude, 0.05 s pulse width, 0.0167 s sampling width, 0.5 s sample period, T = 298 K.
[b] in eV, as calculated by DFT calculation at the B3LYP-D3(BJ)/ZORA-TZ2P level using COSMO to simulate solvent effects.

4.2.6 Discussion

Following absorption of a photon, the excited photosensitizer PS* can be either reduced by the sacrificial electron donor TEOA (reductive quenching) to form PS^-, or oxidized by the HEC cobaloxime (oxidative quenching) to form PS^+. The reduction potential of cobaloxime $E(Co^{III}/Co^{II})$ was found to be located at –0.59 V vs. NHE, and the second reduction $E(Co^{II}/Co^{I})$ was found at –0.74 V vs. NHE in a 1:1 0.1 M pH 7.0 phosphate buffer/MeCN solution (Figure AIII.9), similar as that reported previously.[7] For an oxidative quenching pathway, the potential of the couple involving the triplet excited state of the photosensitizer, $E_{PS*,ox}(PS^+/PS*)$, should be at least more negative than $E(Co^{III}/Co^{II})$ and even than $E(Co^{II}/Co^{I})$, considering that more than 2 electrons are needed to drive hydrogen evolution. With a potential of –0.75 V vs. NHE,

only [Zn-OMeP]$^{4-}$ and [Zn-MeP]$^{4-}$ fulfill this criterion. The other six porphyrin-based photosensitizers are too electron-poor even to be able to proceed with the electron transfer Step 1 (Figure 4.2 right), i.e., reduction of Co^{III} to Co^{II}. The second condition for oxidative quenching, that the ground-state oxidation potential $E_{PS,ox}(PS^+/PS)$ is positive enough to have PS^+ reduced by TEOA, is also met for both [Zn-OMeP]$^{4-}$ and [Zn-MeP]$^{4-}$: the oxidation potential of TEOA was reported to be around 0.82 V vs. NHE,[42] which is lower than the 0.94 V vs. NHE necessary to reduce PS^+ back to PS. In spite of the favorable thermodynamic driving forces, however, none of the two photosensitizers [Zn-OMeP]$^{4-}$ and [Zn-MeP]$^{4-}$ showed any photoactivity for light-driven hydrogen evolution in our conditions. This might be a consequence of unfavorable kinetics at the concentrations used in our experiments, or might be due to short excited-state lifetimes, which have not been determined yet. Overall, photocatalysis seems not to proceed via an oxidative quenching pathway for any of the porphyrin-based photosensitizers in these series.

Since the oxidation potential of TEOA is around 0.82 V vs. NHE,[42] the potentials $E_{PS*,red}(PS*/PS^-)$ for [Zn-OMeP]$^{4-}$, [Zn-MeP]$^{4-}$ and [Zn-F8P]$^{4-}$, are not sufficiently positive for reductive quenching to occur (Step 1 in Figure 4.2 left); only the most electron poor zinc complex [Zn-F16P]$^{4-}$ has a potential of $E_{PS*,red}(PS*/PS^-)$ that is positive enough for reductive quenching to occur. In contrast, all tin porphyrin compounds have a potential $E_{PS*,red}(PS*/PS^-)$ that is high enough for reductive quenching to proceed. However, once reductive quenching has occurred not all photo-reduced porphyrins PS^- offer favorable redox properties to complete the catalytic cycle. Indeed, the PS^- intermediates need to be able to transfer electrons to the HEC as Step 2. According to our data, only the PS^- species of [Zn-F16P]$^{4-}$, [Sn-OMeP]$^{4-}$, and [Sn-MeP]$^{4-}$, have reduction potentials $E_{PS,red}(PS/PS^-)$ that are negative enough to reduce cobaloxime from Co^{III} to Co^{II}, which is necessary for photocatalysis to proceed.

Overall, according to this analysis of redox potentials and the results of photocatalytic HER experiments, the reductive-quenching pathway seems to be the most realistic for the three porphyrin photosensitizers found active in photocatalytic conditions ([Zn-F16P]$^{4-}$, [Sn-OMeP]$^{4-}$, and [Sn-MeP]$^{4-}$). At this point two remarks should be made. First, since the redox properties and estimated excited-state energy of [Sn-OMeP]$^{4-}$ and [Sn-MeP]$^{4-}$ are similar, the low H_2 production obtained with [Sn-OMeP]$^{4-}$ is probably due to its poor photostability. As is clear from Figure 4.4b, the photocatalytic activity of the system containing [Sn-OMeP]$^{4-}$ only lasted 4 h, while for the system containing [Sn-MeP]$^{4-}$ it lasted for more than 20 h. Second, for none of these three active photosensitizers the potential of the photo-reduced PS^- species is sufficiently negative to reduce Co^{II} in cobaloxime to Co^{I}, which is considered to be the H_2-

releasing active species of this catalyst at –0.74 V vs. NHE.[7] Two reasons are proposed here that may explain the hydrogen evolution that is experimentally observed with these three sensitizers. First, in photocatalytic conditions the cobaloxime may decompose into more active HEC species, such as cobalt nanoparticles, characterized by an overpotential η (Figure 4.2) that is lower than that measured in the dark by electrochemistry. Possibly, such species may then be driven by the photo-reduced Zn- and Sn-porphyrin photosensitizers. Second, a TEOA-derived alkyl radical species ($TEOA^{\bullet+}$) forms during the first electron transfer step of the photocatalytic mechanism, which has a lower reduction potential (around –0.79 V vs. NHE in MeCN) than the potential of the PS/PS^{-} couple. This radical may reduce the Co^{II} species of cobaloxime to Co^{I}, further leading to dihydrogen evolution, in a second step that does not involve the formation of a second excited state of the photosensitizer PS*.[7,43] In this hypothesis, light would serve as a way to trigger the reaction and generate the radical $TEOA^{\bullet+}$, and only one photon would be needed per photogenerated molecule of H_2.

4.3 Conclusion

A series of tetra-anionic Zn(II)- and Sn(IV)-porphyrin complexes were prepared and tested as photosensitizers for homogeneous photocatalytic hydrogen evolution in the presence of cobaloxime as the catalyst and TEOA as the sacrificial electron donor in 1:1 pH 7.0 water/acetonitrile solutions. The catalytic activity of the systems containing these photosensitizers appeared to be strongly dependent on the presence of electron-withdrawing or electron-donating substituents on the porphyrin ligand. The Zn(II)-porphyrin complexes in general are more electron rich than the Sn(IV)-porphyrin analogues, and based on our studies we conclude that the reductive-quenching mechanism is followed for all PS molecules. As a consequence, in the Zn series only the electron-poorest complex, $[Zn\text{-}F16P]^{4-}$, was photoactive. It actually showed a very high photostability, as it could work for more than 100 h under green light irradiation without significant decomposition, and showed also the highest PTON (850 after 20 h irradiation) and highest PTOF (59 h^{-1}). For the electron-poorer Sn series, only the most electron-rich compounds of the series, $[Sn\text{-}OMeP]^{4-}$ and $[Sn\text{-}MeP]^{4-}$, appeared to result in a system that was active for HER; photocatalytic activities were lower than with $[Zn\text{-}F16P]^{4-}$, however. Our general understanding of these trends is that the electronic effects introduced by the functional groups on the porphyrin ligands control both their ground-state redox properties and their triplet excited state energies. These effects further control the redox properties of their excited state, and hence their activity when used in photocatalytic systems. We also note that

the oxidation state of the metal plays an important role, too, as Sn(IV) compounds were in average more electron-poor (in the ground state) than those based on Zn(II). This work brings important information for the design of molecular photosensitizers for hydrogen evolution: it demonstrated that a balance between the redox potentials of the ground-state and that of the excited state must be found, which can be fine-tuned by introduction of electron-donating or electron-withdrawing substituents.

4.4 Experimental section

4.4.1 Materials and methods

All reagents were purchased from Sigma-Aldrich and used as received unless otherwise noted. The compounds tetrasodium-5,10,15,20-tetrakis(2,6-dimethoxyphenyl-3-sulfonatophenyl)-21*H*,23*H*-porphyrin ($Na_4[H_2$-OMeP]),[37] tetrasodium-5,10,15,20-tetrakis(2,6-dimethylphenyl-3-sulfonatophenyl)-21*H*,23*H*-porphyrin ($Na_4[H_2$-MeP]),[38] tetrasodium-5,10,15,20-tetrakis(2,6-difluorophenyl-3-sulfonatophenyl)-21*H*,23*H*-porphyrin ($Na_4[H_2$-F8P]),[41] tetrasodium-2,3,7,8,12,13,17,18-octafluoro-5,10,15-20-tetrakis(2,6-difluoro-3-sulfonatophenyl)-21*H*,23*H*-porphyrin ($Na_4[H_2$-F16P]),[40] tetrasodium-5,10,15,20-tetrakis(2,6-difluoro-3-sulfonatophenyl)porphyrin-Zn(II) (Na_4[Zn-F8P]),[41] tetrasodium-2,3,7,8,12,13,17,18-octafluoro-5,10,15-20-tetrakis(2,6-difluoro-3-sulfonatophenyl)porphyrin-Zn(II) (Na_4[Zn-F16P]),[40] were prepared according to published methods. Tetrasodium-5,10,15,20-tetrakis(2,6-dimethoxyphenyl-3-sulfonatophenyl)porphyrin-Zn(II) (Na_4[Zn-OMeP]) and tetrasodium-5,10,15,20-tetrakis(2,6-dimethylphenyl-3-sulfonatophenyl)porphyrin-Zn(II) (Na_4[Zn-MeP]) were prepared according to **Chapter 3**. Cobaloxime and TEOA were purchased from Sigma-Aldrich and used without further treatments. ^{1}H NMR spectra were recorded on a Bruker 400DPX-liq spectrometer operating at 400 MHz. ^{19}F NMR spectra were recorded on a Bruker 500DPX spectrometer operating at 500 MHz. High-resolution mass spectrometric measurements were made on a Bruker Fourier Transform Ion Cyclotron Resonance Mass Spectrometer APEX IV at Leiden University. Elemental analyses were performed at the Mikroanalytisches Laboratorium Kolbe, Germany. Electronic absorption spectra were obtained on a Varian Cary 60 spectrophotometer at 25 °C. The LED optical power was measured using an OPHIR Nova-display laser power meter.

4.4.2 Synthesis

Tetrasodium dichlorido-5,10,15,20-tetrakis(2,6-dimethoxyl-3-sulfonatophenyl)porphyrin stannate(IV) (Na_4[Sn-OMeP])

The ligand $Na_4[H_2$-OMeP] (115 mg, 0.09 mmol) and Milli-Q water (40 mL) were placed under N_2 in a 100 mL round-bottom flask equipped with a magnetic stirring bar and a condenser. A solution of tin(II) chloride heptahydrate (85.3 mg, 0.45 mmol) in Milli-Q water (10 mL) was added to the stirred solution, and the mixture was refluxed for 12 h. After cooling to room temperature, water was rotary evaporated at 40 °C and the residue was redissolved in cold methanol (15 mL). After filtration on a filter paper, methanol was rotary-evaporated, the residue was redissolved in cold methanol (5 mL). The solution was filtered by filter paper, rotary-evaporated, and the crude product was redissolved in Milli-Q water (5 mL) then passed onto an Amberlite IR 120 Na^+ form ion exchange resin column (10 cm length). Washed the resin with 50 mL Milli-Q water and collected the solution, then removed the water by rotary evaporator and the product was further purified on Sephadex-20H size exclusion chromatography to remove excess $SnCl_2$ (methanol). Yield (123 mg, 90%); ^{1}H NMR (400 MHz, CD_3OD): δ = 9.28 – 9.16 (m, 8H; β-pyrrole-H), 8.50 – 8.43 (m, 4H; *p*-Ph-H), 7.44 – 7.28 (m, 4H; *m*-Ph-H), 3.72 – 3.49 (m, 12 H; OCH_3), 3.22 – 2.68 ppm (m, 12 H; OCH_3); HRMS (ESI): *m*/*z* calcd for $C_{52}H_{45}N_4O_{21}S_4Sn^+$: 1309.0483 [*M*-4Na-2Cl+3H+H_2O]$^+$; found: 1309.0483; elemental analysis calcd (%) for $C_{52}H_{40}Cl_2N_4Na_4O_{20}S_4Sn$•$4H_2O$: C 41.02, H 3.18, N 3.68; found: C 40.82, H 3.16, N 3.61. UV-vis (1:1 H_2O/MeCN): λ_{max}(ε in $M^{-1}cm^{-1}$) 423 nm (4.7×10^5), 557 nm (2.2×10^4), 595 nm (5.0×10^3).

Tetrasodium dichlorido-5,10,15,20-tetrakis(2,6-dimethyl-3-sulfonatophenyl)porphyrin stannate(IV) (Na_4[Sn-MeP])

$Na_4[H_2$-MeP]·$9H_2O$ (130 mg, 0.10 mmol) and Milli-Q water (40 mL) were placed under N_2 in a 100 mL round-bottom flask equipped with a magnetic stirring bar and a condenser. A solution of tin(II) chloride (94.8 mg, 0.50 mmol) in Milli-Q water (10 mL) was added to the stirred solution and the mixture was refluxed for 12 h under N_2. After cooling to room temperature, water was rotary evaporated and the residue was redissolved in cold methanol (15 mL). After filtration on a filter paper, methanol was rotary-evaporated, the residue was redissolved in cold methanol (5 mL), the solution was filtered a second time by filter paper and rotary-evaporated, then the crude product was then passed onto an Amberlite IR 120 Na^+ form ion exchange resin column (10 cm length), washed the resin with 50 mL Milli-Q water and collected the solution, then removed the water by rotary evaporator and the product was finally

purified on Sephadex-20H size exclusion chromatography (methanol). Methanol was finally rotary evaporated and the solid dried in vacuo. Yield (128 mg, 92%); ^{1}H NMR (400 MHz, CD_3OD): δ = 9.18 – 9.09 (m, 8H; β-pyrrole-H), 8.43 – 8.38 (m, 4H; *p*-Ph-H), 7.68 – 7.55 (m, 4H; *m*-Ph-H), 2.42 – 2.09 (m, 12H; CH_3), 2.07 – 1.74 ppm (m, 12H; CH_3); HRMS (ESI): *m*/*z* calcd for $C_{52}H_{45}N_4O_{13}S_4Sn^+$: 1181.0882 [*M*-4Na-2Cl+3H+H_2O]$^+$; found: 1181.0881; *m*/*z* calcd for $C_{52}H_{44}N_4NaO_{13}S_4Sn^+$: 1203.0702 [*M*-3Na-2Cl+2H+H_2O]$^+$; found: 1203.0702; elemental analysis calcd (%) for $C_{52}H_{40}Cl_2N_4Na_4O_{12}S_4Sn$•$4H_2O$: C 44.78, H 3.47, N 4.02; found: C 44.97, H 3.43, N 3.96. UV-vis (1:1 H_2O/MeCN): λ_{max}(ε in $M^{-1}cm^{-1}$) 421 nm (5.9×10^5), 556 nm (1.9×10^4), 595 nm (7.3×10^3).

Tetrasodium dichlorido-5,10,15,20-tetrakis(2,6-difluoro-3-sulfonatophenyl)porphyrin stannate(IV) (Na_4[Sn-F8P])

$Na_4[H_2$-F8P]·$4H_2O$ (124 mg, 0.10 mmol) and Milli-Q water (40 mL) were placed under N_2 in a 100 mL round-bottom flask equipped with a magnetic stirring bar and a condenser. A solution of tin(II) chloride (94.8 mg, 0.50 mmol) in Milli-Q water (10 mL) was added to the stirred solution and the mixture was refluxed for 12 h under N_2. After cooling to room temperature, the water was rotary evaporated and the residue was redissolved in cold methanol (15 mL). After filtration over a filter paper, methanol was rotary-evaporated, the residue was redissolved in cold methanol (5 mL), and filtered by filter paper again. The filtrate was rotary-evaporated and the Co-F16 complex was then passed through an Amberlite IR 120 Na^+ form ion exchange resin column (10 cm length) and washed with Milli-Q water before being purified on Sephadex-20H size exclusion chromatography (eluent: methanol). Yield (124 mg, 89%); ^{1}H NMR (400 MHz, CD_3OD): δ = 9.49 – 9.40 (m, 8H; β-pyrrole-H), 8.60 – 8.48 (m, 4H; *p*-Ph-H), 7.72 – 7.61 ppm (m, 4H; *m*-Ph-H); ^{19}F NMR (471 MHz, CD_3OD): δ = -106.42 ppm (d, *J* = 348.2 Hz, 8F; *o*-F); HRMS (ESI): *m*/*z* calcd for $C_{44}H_{21}F_8N_4O_{13}S_4Sn^+$: 1212.8881 [*M*-4Na-2Cl+3H+H_2O]$^+$; found: 1212.8879; *m*/*z* calcd for $C_{44}H_{20}F_8N_4NaO_{13}S_4Sn^+$: 1234.8696 [*M*-3Na+2H+$H_2O$]$^+$; found: 1234.8693; elemental analysis calcd (%) for $C_{44}H_{16}Cl_2F_8N_4Na_4O_{12}S_4Sn$•$2H_2O$: C 38.01, H 1.45, N 4.03; found: C 38.27, H 1.59, N 4.02. UV-vis (1:1 H_2O/MeCN): λ_{max}(ε in $M^{-1}cm^{-1}$) 416 nm (4.4×10^5), 551 nm (1.9×10^4).

Tetrasodium dichlorido-2,3,7,8,12,13,17,18-octafluoro-5,10,15,20-tetrakis(2,6-difluoro-3-sulfonatophenyl)porphyrin stannate(IV) (Na_4[Sn-F16P])

$Na_4[H_2\text{-F16P}]\cdot 5H_2O$ (140 mg, 0.10 mmol) and Milli-Q water (40 mL) were placed under N_2 in a 100 mL round-bottom flask equipped with a magnetic stirring bar and a condenser. A solution of tin(II) chloride (94.8 mg, 0.50 mmol) in Milli-Q water (10 mL) was added to the stirred solution, and the mixture was refluxed for 12 h under N_2. After cooling to room temperature, water was rotary evaporated at 40 °C and the residue was redissolved in cold methanol (15 mL). After filtration on a filter paper, methanol was rotary-evaporated, the residue was redissolved in cold methanol (5 mL). The solution was filtered by filter paper, rotary-evaporated, and the crude product was redissolved in Milli-Q water (5 mL) then passed onto an Amberlite IR 120 Na^+ form ion exchange resin column (10 cm length), the resin washed with Milli-Q water and the product was further purified on Sephadex-20H size exclusion chromatography to remove excess tin(II) chloride (methanol). Yield (133 mg, 87%); ^{1}H NMR (400 MHz, CD_3OD): 8.36 – 8.27 (m, 4H; *p*-Ph-H), 8.43 – 8.35 ppm (m, 4H; *m*-Ph-H); ^{19}F NMR (471 MHz, CD_3OD): δ = -107.17 – -107.83 (m, 4F; *o*-F), -108.40 – -109.14 (m, 4F; *o*-F), -150.19 (s, 4F; β-pyrrole-F), -151.52 ppm (s, 4F; β-pyrrole-F); HRMS (ESI): *m*/*z* calcd for $C_{44}H_{13}F_{16}N_4O_{13}S_4Sn^+$: 1356.8127 [*M*-4Na-2Cl+3H+H_2O]$^+$; found: 1356.8123; elemental analysis calcd (%) for $C_{44}H_8Cl_2F_{16}N_4Na_4ZnO_{12}S_4Sn\bullet 2H_2O$: C 34.44, H 0.79, N 3.65; found: C 34.46, H 0.72, N 3.64. UV-vis (1:1 H_2O/MeCN): λ_{max}(ε in $M^{-1}cm^{-1}$) 411 nm (3.1×10^5), 544 nm (2.2×10^4), 615 nm (4.8×10^3).

4.4.3 Electrochemistry

Differential pulse voltammetry (DPV) measurements were performed using an Autolab PGstart10 potentiostat controlled by GPES4 software. All the DPV measurements were recorded in 1:1 0.1 M pH 7.0 sodium phosphate buffer/acetonitrile solution using a three-compartment cell possessing a 0.07 cm^2 glassy-carbon electrode as the working electrode, Pt wire as the auxiliary electrode, Ag/AgCl (saturated KCl aq.) as the reference electrode, and $K_3[Fe(CN)_6]$ was added at the end of the measurements as internal standard (E($[Fe(CN)_6]^{3-}$/$[Fe(CN)_6]^{4-}$) = +0.361 V vs NHE).[44] Unless otherwise indicated, all potentials were converted to the scale relative to NHE. The solutions were bubbled with high-purity argon for at least 15 min before running DPV.

4.4.4 Photo-induced hydrogen evolution

Photo-induced hydrogen evolution from water was analysed by a hydrogen electrode (Unisense H2-NP) controlled by x-5 UniAmp using Logger software. The irradiation source

was an OSRAM Opto Semiconductors LD W5SM LED (λ_{irr} 550 nm, 9 mW) with water cooling. All the photochemical hydrogen evolution measurements were carried out in a thermostatic (298 K) photochemical reactor (total volume 25.0 mL). The photosensitizer Na_4[Zn-OMeP] •4H_2O (0.04 mM, 0.17 mg), Na_4[Zn-MeP]•H_2O (0.04 mM, 0.15 mg), Na_4[Zn-F8P]•3H_2O (0.04 mM, 0.15 mg), Na_4[Zn-F16P]•5H_2O (0.04 mM, 0.18 mg), Na_4[Sn-OMeP]•4H_2O (0.04 mM, 0.18 mg), Na_4[Sn-MeP]•4H_2O (0.04 mM, 0.17 mg), Na_4[Sn-F8P]•2H_2O (0.04 mM, 0.17 mg), or Na_4[Sn-F16P]•2H_2O (0.04 mM, 0.18 mg) and the catalyst cobaloxime (0.49 mM, 0.60 mg) were added as solids in the reactor, and dissolved using 1.5 mL 10% (v/v) TEOA aqueous solution neutralized with concentrated HCl to pH 7.0, and 1.5 mL acetonitrile. Under constant stirring, the reactor was equipped with 1 rubber septum and 2 silicon septa in order to make an air-tight system (the set-up is shown in Figure AI.29). The hydrogen electrode was then inserted through the septum, to measure the hydrogen concentration in the head space (gas phase) of the photochemical reactor, and the whole system was deaerated by high-purity argon bubbling through the solution for at least 15 min. After removing the needle bringing argon, the hydrogen electrode was calibrated by a four-time injection of 100 µL (4.46 µmol at 1 atm) of high-purity H_2 into the closed system; the calibration was adapted with the pressure change using Logger software, affording direct reading of the volume of dihydrogen (µL) produced in the gas phase of the reactor (V_{gas} = 22.0 mL). Following calibration, the three used septa were replaced by new ones and the hydrogen electrode was again inserted into the system. The system was degassed for 15 min with argon, then data recording was started, first keeping the system in the dark for 30 min prior to starting light irradiation. Unless otherwise indicated, the data recording was stopped after 22 h of light irradiation.

4.4.5 Photocatalytic turnover number and turnover frequency determination

The experimental dihydrogen evolution was determined by a hydrogen electrode (Unisense OX-NP) controlled by x-5 UniAmp using Logger software. The amount of H_2 formed during illumination was used to calculate the photocatalytic turnover number (PTON) using the following equation:

$$PTON = \frac{n_{H_2}}{n_{PS}}$$

in which n_{H_2} is the number of mol of hydrogen calculated from the volume of the dioxygen produced in the photocatalytic experiment as indicated by the calibrated hydrogen electrode in

the gas phase (µL), divided by 22.4 L/mol, and n_{PS} is the number of mol of Zn- or Sn-porphyrin complex used in the photocatalytic experiment.

The maximum photocatalytic turnover frequency PTOF (in h^{-1}) for photocatalytic hydrogen evolution was obtained using Origin 9.1 software by 1) nonlinear curve fitting of the time evolution of the PTON, starting at t = 30 min for photocatalytic reactions (category: Growth/Sigmoidal, function: logistic Fit); 2) calculating the first time derivative PTOF = f(t) of the PTON = g(t) function using mathematics, differentiate, and 3) identify the maximum value of PTOF = f(t) (an example for $[Sn\text{-}MeP]^{4-}$ is shown in Figure 4.7).

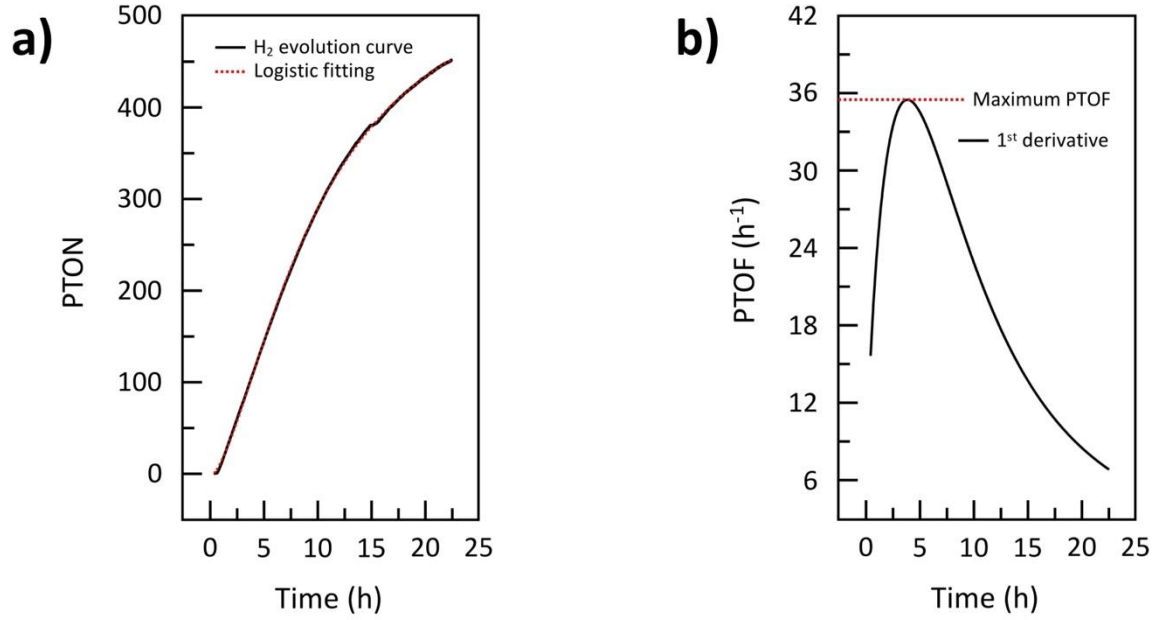

Figure 4.7 *Calculation of maximum PTOF of the* $[Sn\text{-}MeP]^{4-}$ *based photocatalytic hydrogen evolution system.*

4.4.6 Density functional theory calculations

All density functional theory (DFT) calculations were performed within the AMS2020 package published by SCM.[45] The X,Y,Z geometries of the ground-state singlet and lowest triplet excited states of each complex were optimized using the (GGA-type) OPBE density functional approximation,[46] projected onto a triple-ζ polarized (TZP) Slater-type basis set, including scalar relativistic effects by means of the zero-order regular approximation (ZORA).[47] To speed up the calculations, the 1S electrons of C, N ,O, F, S and Cl, the 1S-2P electrons for Zn, and the 1S-4P electrons for Sn were frozen. Grimme3 BJDAMP (-D3(BJ)) dispersion corrections were used.[48] Water solvation was modelled implicitly via the conductor-like screening model (COSMO).[49,50]

The energies of the obtained geometries were then re-evaluated by performing a single-point calculation, employing the (hybrid) B3LYP-D3(BJ) functional[51-54] in a ZORA triple-ζ Slater-type basis with two polarization functions (ZORA-TZ2P). Again, the COSMO model was employed to account for solvent effects.

4.5 Acknowledgement

T. de Haas and Dr. F. Buda are wholeheartedly acknowledged for performing the DFT calculations. C. Liu gratefully acknowledges the China Scholarship Council (CSC) for a personal grant (No. 201706360150).

4.6 References

[1] K. E. Dalle, J. Warnan, J. J. Leung, B. Reuillard, I. S. Karmel, E. Reisner, *Chem. Rev.* **2019**, *119*, 2752-2875.
[2] A. Mazzeo, S. Santalla, C. Gaviglio, F. Doctorovich, J. Pellegrino, *Inorg. Chim. Acta* **2021**, *517*, 119950.
[3] W. Zhang, W. Lai, R. Cao, *Chem. Rev.* **2017**, *117*, 3717-3797.
[4] A. Pannwitz, D. M. Klein, S. Rodriguez-Jimenez, C. Casadevall, H. Song, E. Reisner, L. Hammarstrom, S. Bonnet, *Chem. Soc. Rev.* **2021**, *50*, 4833-4855.
[5] W. T. Eckenhoff, *Coord. Chem. Rev.* **2018**, *373*, 295-316.
[6] Y. J. Yuan, Z. T. Yu, D. Q. Chen, Z. G. Zou, *Chem. Soc. Rev.* **2017**, *46*, 603-631.
[7] E. Giannoudis, E. Benazzi, J. Karlsson, G. Copley, S. Panagiotakis, G. Landrou, P. Angaridis, V. Nikolaou, C. Matthaiaki, G. Charalambidis, E. A. Gibson, A. G. Coutsolelos, *Inorg. Chem.* **2020**, *59*, 1611-1621.
[8] J. I. Goldsmith, W. R. Hudson, M. S. A. Lowry, T. H. , S. Bernhard, *J. Am. Chem. Soc.* **2005**, *127*, 7502-7510.
[9] S. Chakraborty, E. H. Edwards, B. Kandemir, K. L. Bren, *Inorg. Chem.* **2019**, *58*, 16402-16410.
[10] A. Reynal, E. Pastor, M. A. Gross, S. Selim, E. Reisner, J. R. Durrant, *Chem. Sci.* **2015**, *6*, 4855-4859.
[11] C.-F. Leung, S.-M. Ng, C.-C. Ko, W.-L. Man, J. Wu, L. Chen, T.-C. Lau, *Energy Environ. Sci.* **2012**, *5*, 7903-7907.
[12] A. Call, Z. Codola, F. Acuna-Pares, J. Lloret-Fillol, *Chem. Eur. J.* **2014**, *20*, 6171-6183.
[13] P. Du, K. Knowles, R. Eisenberg, *J. Am. Chem. Soc.* **2008**, *130*, 12576-12577.
[14] X. Wang, S. Goeb, Z. Ji, N. A. Pogulaichenko, F. N. Castellano, *Inorg. Chem.* **2011**, *50*, 705-707.
[15] B. Probst, A. Rodenberg, M. Guttentag, P. Hamm, R. Alberto, *Inorg. Chem.* **2010**, *49*, 6453-6460.
[16] A. Rodenberg, M. Orazietti, B. Probst, C. Bachmann, R. Alberto, K. K. Baldridge, P. Hamm, *Inorg. Chem.* **2015**, *54*, 646-657.
[17] W. P. To, G. S. Tong, W. Lu, C. Ma, J. Liu, A. L. Chow, C. M. Che, *Angew. Chem. Int. Ed.* **2012**, *51*, 2654-2657.
[18] O. S. Wenger, *Chem. Rev.* **2013**, *113*, 3686-3733.
[19] O. S. Wenger, *J. Am. Chem. Soc.* **2018**, *140*, 13522-13533.
[20] F. Glaser, O. S. Wenger, *Coord. Chem. Rev.* **2020**, *405*, 213129.
[21] J. Wang, C. Li, Q. Zhou, W. Wang, Y. Hou, B. Zhang, X. Wang, *Dalton Trans.* **2015**, *44*, 17704-17711.
[22] Q. Deng, Y. Xu, Z. Wang, T. Miao, X. Fu, L. Xu, *J. Phys. Chem. C* **2019**, *123*, 30351-30359.
[23] P. Zhang, M. Wang, J. Dong, X. Li, F. Wang, L. Wu, L. Sun, *J. Phys. Chem. C* **2010**, *114*, 15868-15874.
[24] C.-B. Li, P. Gong, Y. Yang, H.-Y. Wang, *Catal. Lett.* **2018**, *148*, 3158-3164.
[25] C. Zhang, G. Li, X. Cai, *Int. J. Energy Res.* **2018**, *42*, 977-984.
[26] Y. Zhao, Y. Wang, Q. Wu, J. Lin, S. Wu, W. Hou, R. Wu, G. Luo, *Chinese J. Catal.* **2018**, *39*, 517-526.
[27] A. Edel, P. A. Marnot, J. P. Sauvage, *Nouv. J. Chim.* **1984**, *8*, 495-498.
[28] S. P. Luo, E. Mejia, A. Friedrich, A. Pazidis, H. Junge, A. E. Surkus, R. Jackstell, S. Denurra, S. Gladiali, S. Lochbrunner, M. Beller, *Angew. Chem. Int. Ed.* **2013**, *52*, 419-423.
[29] S. Fischer, D. Hollmann, S. Tschierlei, M. Karnahl, N. Rockstroh, E. Barsch, P. Schwarzbach, S.-P. Luo, H. Junge, M. Beller, S. Lochbrunner, R. Ludwig, A. Brückner, *ACS Catal.* **2014**, *4*, 1845-1849.
[30] M. Karnahl, E. Mejía, N. Rockstroh, S. Tschierlei, S.-P. Luo, K. Grabow, A. Kruth, V. Brüser, H. Junge,

S. Lochbrunner, M. Beller, *ChemCatChem* **2014**, *6*, 82-86.
[31] R. S. Khnayzer, C. E. McCusker, B. S. Olaiya, F. N. Castellano, *J. Am. Chem. Soc.* **2013**, *135*, 14068-14070.
[32] E. Mejia, S. P. Luo, M. Karnahl, A. Friedrich, S. Tschierlei, A. E. Surkus, H. Junge, S. Gladiali, S. Lochbrunner, M. Beller, *Chem. Eur. J.* **2013**, *19*, 15972-15978.
[33] K. Ladomenou, M. Natali, E. Iengo, G. Charalampidis, F. Scandola, A. G. Coutsolelos, *Coord. Chem. Rev.* **2015**, *304-305*, 38-54.
[34] A. Panagiotopoulos, K. Ladomenou, D. Sun, V. Artero, A. G. Coutsolelos, *Dalton Trans.* **2016**, *45*, 6732-6738.
[35] N. Queyriaux, E. Giannoudis, C. D. Windle, S. Roy, J. Pécaut, A. G. Coutsolelos, V. Artero, M. Chavarot-Kerlidou, *Sustain. Energy Fuels* **2018**, *2*, 553-557.
[36] T. Lazarides, M. Delor, I. V. Sazanovich, T. M. McCormick, I. Georgakaki, G. Charalambidis, J. A. Weinstein, A. G. Coutsolelos, *Chem. Commun.* **2014**, *50*, 521-523.
[37] C. Liu, D. van den Bos, B. den Hartog, D. van der Meij, A. Ramakrishnan, S. Bonnet, *Angew. Chem. Int. Ed.* **2021**, *60*, 13463-13469.
[38] M. F. Zipplies, W. A. Lee, T. M. Bruice, *J. Am. Chem. Soc.* **1986**, *108*, 4433-4445.
[39] S. Nakagaki, F. L. Benedito, F. Wypych, *J. Mol. Catal. A Chem.* **2004**, *217*, 121-131.
[40] J. C. Biffinger, H. Sun, A. P. Nelson, S. G. DiMagno, *Org. Biomol. Chem.* **2003**, *1*, 733-736.
[41] A. Sułek, B. Pucelik, J. Kuncewicz, G. Dubin, J. M. Dąbrowski, *Catal. Today* **2019**, *335*, 538-549.
[42] Y. Pellegrin, F. Odobel, *C. R. Chim.* **2017**, *20*, 283-295.
[43] D. D. M. Wayner, J. J. Dannenberg, D. Griller, *Chem. Phys. Lett.* **1986**, *131*, 189-191.
[44] R. C. J. Murray, P. A. Rock, *Electrochim. Acta* **1968**, *13*, 969-975.
[45] AMS. SCM, Theoretical Chemistry, Vrije Universiteit: Amsterdam, The Netherlands.
[46] M. Swart, A. W. Ehlers, K. Lammertsma, *Mol. Phys.* **2004**, *102*, 2467–2474.
[47] E. Van Lenthe, *J. Chem. Phys.* **1999**, *110*, 8943–8953.
[48] S. Grimme, S. Ehrlich, L. Goerigk, *J. Comput. Chem.* **2011**, *32*, 1456–1465.
[49] A. Klamt, *J. Phys. Chem.* **1995**, *99*, 2224–2235.
[50] A. Klamt, V. Jonas, *J. Chem. Phys.* **1996**, *105*, 9972–9981.
[51] A. D. Becke, *J. Chem. Phys.* **1993**, *98*, 1372–1377.
[52] A. D. Becke, *Phys. Rev. A* **1988**, *38*, 3098.
[53] S. H. Vosko, L. Wilk, M. Nusair, *Can. J. Phys.* **1980**, *58*, 1200–1211.
[54] P. J. Stephen, F. J. Devlin, C. F. Chabalowski, M. J. Frisch, *J. Phys. Chem.* **1994**, *98*, 11623–11627.